THE JOURNAL OF PHYSICAL CHEMISTRY B

Article

pubs.acs.org/JPCB

Fluorescence Detection of Lipid-Induced Oligomeric Intermediates Involved in Lysozyme "Amyloid-Like" Fiber Formation Driven by Anionic Membranes

Ana M. Melo,[†] Joana C. Ricardo,[†] Aleksander Fedorov,[†] Manuel Prieto,[†] and Ana Coutinho*[,†,‡]

[†]Centro de Química-Física Molecular and Institute of Nanoscience and Nanotechnology, I.S.T, Universidade Técnica de Lisboa, Av. Rovisco Pais, 1049-001 Lisboa, Portugal

[‡]Dep. Química e Bioquímica, FCUL, Campo Grande, 1749-016 Lisboa, Portugal

Supporting Information

ABSTRACT: Recent findings implicate that "amyloid-like" fiber formation by several non-amyloidogenic proteins/peptides can be triggered by negatively charged lipid membranes. In order to elucidate the factors that govern the formation of these structures, the interaction of lysozyme with phosphatidylserine-containing lipid vesicles was studied by steady-state and time-resolved fluorescence measurements. Three consecutive stages in the interaction of Alexa488-fluorescently labeled lysozyme (Lz-A488) with acidic lipid vesicles were identified in ensemble average measurements. The variation of the mean fluorescence lifetime of Lz-A488 as a function of the surface coverage of the liposomes was quantitatively described by a cooperative partition model that assumes that monomeric lysozyme molecules partition into the bilayer surface and reversibly assemble into oligomers with k subunits ($k \geq 6$). The global fit to the experimental data covering a wide range of experimental conditions was performed by taking into account electrostatic effects by means of the Gouy−Chapman theory using a single self-consistent pair of parameters (aggregation constant and stoichiometry). The lipid−protein supramolecular assemblies formed at a low lipid/protein molar ratio were further characterized by fluorescence lifetime imaging microscopy at the single-fiber level, which reported that quenched oligomers are the predominant species in these structures.

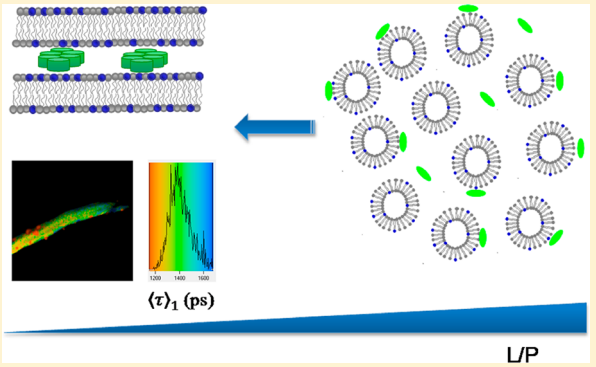

INTRODUCTION

The protein/peptide self-assembly into highly ordered β-sheet-rich fibrils plays a key role in various serious pathologies, including Alzheimer's and Parkinson's diseases and type II diabetes mellitus.[1,2] However, the ability of proteins/peptides to form amyloid fibrils is not restricted to amyloidogenic sequences. It has been shown that many non-amyloidogenic proteins/peptides also form "amyloid-like" fibrils *in vitro* under specific conditions of pH, temperature, and ionic strength.[3,4] Therefore, it seems consensual that protein/peptide aggregation does not depend only on the polypeptide sequence but also on external conditions.[5] Increasing evidence supports that biological membranes have a key role in triggering protein/peptide fibrillation by acting as a two-dimensional catalyst.[6−8] Specifically, it has been suggested that the initial binding of amyloidogenic precursors to anionic membranes can promote the pathological conversion into amyloidogenic assemblies by the establishment of electrostatic interactions between the negatively charged lipid groups and clusters of basic groups on the proteins or peptides.[6,7] Additionally, it has been reported that oligomeric intermediate species of amyloidogenic peptides or proteins might be the primary cytotoxicity agents contributing to cell damage and toxicity.[8−10] Therefore, the identification and characterization of oligomeric species and the factors that lead to their formation will be crucial for designing new therapies for the treatment of these pathologies.

More recently, Kinnunen and co-workers have also proposed that membranes containing negatively charged phospholipids can trigger rapid "amyloid-like" fiber formation by several non-amyloidogenic proteins, such as hen egg-white lysozyme (HEWL), myoglobin, and cytochrome *c* under nearly physiological conditions.[11] Further studies by this group extended these observations to other non-amyloidogenic proteins/peptides such as endostatin (an inhibitor of tumor angiogenesis and growth),[12] different antimicrobial peptides,[12−16] and phospholipase A_2.[17,18] In order to elucidate the key factors that govern the formation of these lipid−protein supramolecular mixed assemblies, HEWL was used here as a model non-amyloidogenic protein. This enzyme is one of the most extensively studied model proteins, whose structure and physicochemical properties have been well characterized.[19] HEWL has been widely used to study the mechanism of

Received: October 19, 2012
Revised: December 10, 2012
Published: January 17, 2013

   dx.doi.org/10.1021/jp310396v | *J. Phys. Chem. B* 2013, 117, 2906−2917

amyloid aggregation *in vitro*.[19] Additionally, this protein is homologous to human lysozyme, the variants of which have been shown to form amyloid fibrils, implicated in hereditary systemic amyloidosis.[20,21] The biological functions of lysozyme, including its antimicrobial, antitumor, and immune-modulatory activities, have been suggested to be related to its lipid-binding properties and subsequent capacity to disrupt membranes.[22] In fact, it has been found that the denatured[23] and mutated[24,25] forms of the protein, which lack enzymatic activity, also display a bactericidal action. This enzyme (pI = 11) has a very strong affinity to negatively charged phospholipid vesicles[26] due to the critical role of electrostatic interactions on its membrane binding, which depends on the pH, ionic strength of the medium, and molar fraction of negatively charged phospholipids.[26−32] Although a great deal is known about lysozyme interactions with anionic lipid membranes, the molecular mechanism of its misfolding and self-assembly induced by negatively charged surfaces has not been characterized in detail. To gain further insight into these molecular events, an external fluorescent label was introduced in lysozyme by reacting the ε-amino groups of its lysine residues with Alexa Fluor 488 (A488), a very bright fluorophore that is insensitive to pH in the physiological range. When covalently linked to a protein, Alexa dyes can often be used as sensitive reporters for folding transitions due to their sensitivity to a photon-induced electron transfer (PET)-based quenching mechanism.[33,34] In fact, the protein conjugates of these dyes frequently exhibit complex fluorescence intensity decays due to conformation-sensitive collisional quenching caused by contact interactions with nearby electron-donating amino acid residues (mainly Trp residues).[35−37] We took advantage of this property to track distinct subpopulations of Alexa488-fluorescently labeled lysozyme (Lz-A488) produced by sequential conformational/oligomerization changes upon its binding to anionic lipid membranes by measuring the variation of its fluorescence properties using both steady-state and time-resolved fluorescence techniques. Furthermore, these changes were also related to the mesoscopic structural alterations undergone by the lipid vesicles in the presence of the protein. The variations in the amplitude-weighted mean fluorescence lifetime of Lz-A488 measured in these ensemble average studies were quantitatively described by a three-state model that considers lysozyme partition coupled to its oligomerization in the anionic liposomes. By taking into account the electrostatic effects according to the Gouy−Chapman theory,[38] Lz-A488 was found to assemble into a multimeric species (k-mers with $k \geq 6$) that characteristically presented a mean fluorescence lifetime shorter than the free and membrane-bound monomeric Lz-A488 species. Complementary studies performed at the single-fiber level by fluorescence lifetime imaging microscopy (FLIM) confirmed that Lz-A488 also forms fluorescent quenched oligomers in these lipid−protein mixed assemblies formed at a low lipid-to-protein (L/P) molar ratio, which have been proposed earlier to be "amyloid-like" fibrils.[11]

MATERIALS AND METHODS

Materials. 1-Palmitoyl-2-oleoyl-*sn*-glycero-3-phosphocholine (POPC), 1-palmitoyl-2-oleoyl-*sn*-glycero-3-phosphoserine (POPS), and 1,2-dioleoyl-*sn*-glycero-3-phosphoethanolamine-*N*-(lissamine rhodamine B sulfonyl) (Rhod-DOPE) were obtained from Avanti Polar Lipids (Alabaster, AL). Lysozyme (EC 3.2.1.17) from chicken egg-white was purchased from Fluka Biochemika (Buchs, Switzerland). A488 succinimidyl ester (SE) (carboxylic acid, succinimidyl ester, mixed isomers, dilithium salt) was obtained from Molecular Probes, Invitrogen (Eugene, OR). Other chemicals were of analytical or spectroscopic reagent grade, and were used without any purification.

Fluorescent Labeling of Lysozyme. Lysozyme was covalently labeled with A488 SE dye on its amine groups at pH 8.3 essentially as previously described, using either an equimolar or a 2-fold molar excess of the dye relative to the protein.[26] Lz-A488 was separated from unreacted free probe by gel filtration through a Sephadex G-25 gel filtration column equilibrated in 20 mM HEPES-KOH, 0.1 mM EDTA, pH 7.4 buffer. The final dye-to-protein molar ratio, D/P, of each labeling batch was determined spectrophotometrically using the extinction coefficient of the dye provided by the supplier[39] and that of lysozyme in the UV.[40]

Liposome Preparation. Large unilamellar vesicles (LUVs) containing POPC mixtures with 20 or 30 mol % POPS were prepared by extrusion of lipid dispersions through 100 nm pore diameter polycarbonate membranes using 20 mM HEPES−KOH, 0.1 mM EDTA, pH 7.4 buffer.[26] For confocal microscopy studies, Rhod-DOPE was cosolubilized in the lipid mixture at 1:1000 molar ratio. The concentration of phospholipid stock solutions was determined using phosphate analysis.[41]

Sample Preparation. Each sample used for steady-state and time-resolved fluorescence measurements (ensemble average) was prepared independently, and its L/P molar ratio was varied within a wide range in two different ways: either a fixed total Lz-A488 concentration (0.5 or 3.0 μM) was added to different total phospholipid concentrations ($0 < [L]_t < 6$ mM), or different protein concentrations (0−9 μM) were added to the liposomes at 0.86 mM total phospholipid concentration. In all assays, the liposome suspensions were incubated with the protein at least 1 h at room temperature prior to measurements.

Preparation of the Lipid−Protein Fibers (Supramolecular Complexes) Formed at a Low L/P Ratio. The lipid−protein supramolecular mixed assemblies formed at a low L/P ratio were obtained by incubating 6 μM lysozyme (nonlabeled or fluorescently labeled with A488 with a final D/P = 0.67) with 100 μM POPC:POPS 80:20 LUVs (with or without 1:1000 mol/mol Rhod-DOPE) under constant magnetic stirring with a micro stir bar for 2 h. The samples were then centrifuged at 10 000g for 20 min, and the supernatant was gently removed to be imaged by confocal laser scanning microscopy (CLSM) or FLIM.

Absorption and Steady-State Fluorescence Measurements. Absorption measurements were carried out at room temperature using a Shimadzu MPC-3100 spectrophotometer (Shimadzu Scientific Instruments, Columbia, MD). Fluorescence measurements were performed in an SLM-AMINCO 8100 spectrofluorometer (SLM Instruments Inc., Urbana, IL) with double excitation and emission monochromators, fitted with automated rotating Glan-Thompson polarizers, and operating in "photon counting" mode. The emission spectra of the samples (λ_{exc} = 480 nm) were measured in 5 × 5 mm path length quartz cuvettes, with excitation and emission bandwidths of 4 and 8 nm, respectively, and with the emission polarizer set at the magic angle (54.7°). Background intensities arising from the lipid vesicles were always taken into account.

Liposome Aggregation Measurements. Protein-mediated aggregation of liposomes was determined from the change in pseudoabsorbance or 90° light scattering, which follows the

dx.doi.org/10.1021/jp310396v | J. Phys. Chem. B 2013, 117, 2906−2917

increase in turbidity of the liposome suspension upon addition of Lz-A488. Absorbance was measured at 360 nm in a spectrophotometer, and right-angle light scattering was observed in a spectrofluorometer with the excitation and emission wavelengths set at 650 nm (4 nm bandwidths).

Time-Resolved Fluorescence Measurements. Time-resolved fluorescence intensity measurements were performed by the single-photon timing technique as previously described.[42] The samples were excited using a synchronously pumped, frequency doubled, Ti-sapphire laser. The fluorescence decays, $I(t)$, were measured with an emission polarizer set at the magic angle (54.7°) relative to the vertically polarized excitation beam (λ_{exc} = 460 nm). The fluorescence was detected at 515 nm using a Jobin-Yvon HR320 monochromator in combination with a cutoff filter to avoid interference from Rayleigh-scattered light and using a Hamamatsu R-2809U microchannel plate photomultiplier. The instrument response function was recorded as excitation light scattered by a Ludox solution (silica, colloidal water solution, Aldrich, Milwaukee, WI). The data were collected in a multichannel analyzer with a time window of 1024 channels, at typically 15.3−16.8 ps/channel, up to 50 000 and 20 000 counts in the peak channel of the instrument response function and decay curves, respectively. Details about the fluorescence decay analysis can be found in the Supporting Information.

Confocal Laser Scanning Microscopy. Confocal images were acquired using a Leica TCS SP5 (Leica Microsystems CMS GmbH, Manheim, Germany) inverted microscope (DMI6000) with 63× water (1.2 numerical aperture) apochromatic objective (Zeiss, Jena Germany). Argon lines at 488 and 514 nm were used for Lz-A488 and Rhod-DOPE excitation, respectively. The Lz-A488 emission was collected from 500 to 580 nm, while Rhod-DOPE was acquired in the 530−680 nm range.

Fluorescence Lifetime Imaging Microscopy. FLIM was performed using a Becker & Hickl setup (Berlin, Germany) in combination with the confocal microscope. 760 nm two-photon excitation (TPE) was used to excite the fluorescently labeled protein present in the lipid−protein supramolecular assemblies. TPE pulses were generated by a Ti:sapphire laser (Spectra-Physics Mai Tai BB, 710−990 nm) with a pulse frequency of 80 MHz. The emission light from the samples was further selected with a 500−550 nm band-pass filter (Chroma Technology Corp., Rockingham, USA) and recorded using a PMC-100-4 cooled high speed PMT detection head (Becker & Hickl). Images with a frame size of 128 × 128 pixels were acquired using a Becker & Hickl SPC 830 module. The average count rate was 10^3−10^4 counts/s, and 250 s of scanning time was used for image acquisition. Details about the fluorescence decay analysis can be found in the Supporting Information.

Cooperative Partition Model Combined with the Gouy−Chapman Theory. As described in the Results and Discussion section, three consecutive stages were identified in the interaction of Lz-A488 with POPC LUVs containing variable mol % POPS, but for the sake of simplicity, our quantitative description of this system only considers two coupled equilibria (Scheme 1). Briefly, monomeric lysozyme is assumed to distribute between the aqueous and membrane phases (negatively charged liposomes) according to a simple partitioning equilibrium:[43]

Scheme 1. Interaction of Lysozyme with Anionic Lipid Vesicles[a]

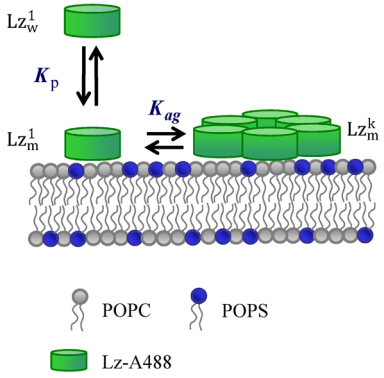

[a]Three-state model of lysozyme interaction with POPS-containing liposomes: coupled equilibria of lysozyme partition and reversible assembly into membrane-bound lysozyme oligomers (k-mers). See the text for more details.

$$K_p^{FCS} = \frac{\frac{[Lz_m^1]}{[L]_{ac}}}{\frac{[Lz_w^1]}{[W]}} \quad (1)$$

where K_p^{FCS} is the mole-fraction partition coefficient previously determined for Lz-A488 using FCS[26] and $[Lz_m^1]$ and $[Lz_w^1]$ are the molar concentrations of membrane-bound and aqueous monomeric lysozyme, respectively. $[L]_{ac}$ and $[W]$ are the accessible lipid (half of total lipid concentration) and water concentrations, respectively. At high liposome coverage, membrane-bound lysozyme reversibly assembles into oligomers containing k subunits according to a discrete oligomerization equilibrium described by the surface aggregation constant, K_{ag}:

$$K_{ag} = \frac{\frac{[Lz_m^k]}{[L]_{ac}}}{\left(\frac{[Lz_m^1]}{[L]_{ac}}\right)^k} \quad (2)$$

where $[Lz_m^k]$ is the molar concentration of the membrane-bound k-meric form of lysozyme.

As expected for a mainly electrostatic-driven interaction, ln K_p^{FCS} varied linearly with ψ_o, the surface potential of the lipid vesicles prepared with a variable molar fraction of POPS, x_{POPS} (Supporting Information, Figure S1). This parameter, which is related to the charge of the bilayer (surface charge density), σ, due to the anionic phospholipid POPS with a charge z_{POPS}, was calculated using the Gouy−Chapman theory[38] by iteratively finding a solution for ψ_o that allowed the numerical values of eqs 3 and 4 to be identical:

$$\sigma = \sqrt{2000\varepsilon_o\varepsilon_r RT \sum_i C_{i,eq}(e^{-z_i F_o \psi_o/RT} - 1)} \quad (3)$$

$$\sigma = \frac{e_o}{A_{PL}}(z_{POPS}x_{POPS}) \quad (4)$$

In these equations, $C_{i,eq}$ is the concentration of the ith electrolyte in the bulk aqueous phase, z_i is the valency of the ith species, and the physical constants have the usual meaning. A value of 0.65 nm^2 was used for the average surface area of each phospholipid, A_{PL}.[44] The corrected partition coefficient, K_p^{cor}, that considers the screening of the interfacial membrane charge

dx.doi.org/10.1021/jp310396v | J. Phys. Chem. B 2013, 117, 2906−2917

due to the progressive binding of the cationic conjugated protein with an effective charge z_p, to the anionic lipid vesicles is given by

$$K_p^{cor} = K_p^{FCS} \exp[m(\psi_o^{cor} - \psi_o)] \quad (5)$$

where m measures the dependence of $\ln K_p^{FCS}$ with ψ_o (Supporting Information, Figure S1) and ψ_o^{cor} is the corrected surface potential. In this case, the surface charge density of the lipid vesicles was calculated according to eq 6 by assuming that the available membrane surface is independent of protein concentration:

$$\sigma = \frac{e_o}{A_{PL}}\left(z_{POPS}x_{POPS} + z_p\left(\frac{[Lz_m^1] + k[Lz_m^k]}{[L]_{ac}}\right)\right) \quad (6)$$

For any set of experimental conditions, both the partition and oligomerization equilibria must be obeyed simultaneously (Scheme 1). Combining eqs 1 and 2 with the protein mass balance equation in monomer units

$$[Lz]_t = [Lz_w^1] + [Lz_m^1] + k[Lz_m^k] \quad (7)$$

and further taking into account the electrostatic effects implicit in eq 5 results in

$$kK_{ag}[L]_{ac}^{(1-k)}[Lz_m^1]^k + \left(1 + \frac{[W]}{K_p^{cor}[L]_{ac}}\right)[Lz_m^1] - [Lz]_t = 0 \quad (8)$$

where $[Lz]_t$ represents the total concentration of lysozyme in the system. Equation 8 is a polynomial of kth order that has no general analytical solution, and therefore, it has to be solved numerically using an iterative method. For each set of predefined numerical values of k and K_{ag}, guesses for the membrane-bound Alexa488-lysozyme monomer concentration, $[Lz_m^1]$, and surface potential, ψ_o^{cor}, were initially made. The corresponding charge density of the membrane, σ, was calculated according to eq 3 and its value compared to the one obtained using eq 6. The sum of their square deviations was then minimized using the routine Solver from Microsoft Office Excel 2010 in an iterative procedure by varying the initial guesses of ψ_o^{cor} and $[Lz_m^1]$. The solution obtained for eq 8 was then used to calculate the mole fractions of the different lysozyme populations present in each sample, namely, the mole fractions of aqueous and membrane-bound monomeric lysozyme ($x_{Lz_w^1}$ and $x_{Lz_m^1}$, respectively) and oligomeric lysozyme ($x_{Lz_m^k}$).

The amplitude-weighted mean fluorescence lifetime, $\langle\tau\rangle_1$, of Lz-A488 in the presence of liposomes is a population average of its characteristic values in the aqueous ($\langle\tau\rangle_1^{w1}$) and membrane-bound monomeric and k-meric states ($\langle\tau\rangle_1^{m1}$ and $\langle\tau\rangle_1^{mk}$, respectively):

$$\langle\tau\rangle_1^{calc} = x_{Lz_w^1}\langle\tau\rangle_1^{w1} + x_{Lz_m^1}\langle\tau\rangle_1^{m1} + kx_{Lz_m^k}\langle\tau\rangle_1^{mk} \quad (9)$$

Therefore, the three-state cooperative partition model proposed for lysozyme interaction with the lipid vesicles could be fitted to the experimental data of $\langle\tau\rangle_1^{exp}$ through finding a pair of values for k and K_{ag} that simultaneously minimized the mean-square deviation (MSD) function:

$$MSD = \sum_{i=1}^{n} (\langle\tau\rangle_1^{exp} - \langle\tau\rangle_1^{calc})^2/\nu \quad (10)$$

where n and ν are the number of experimental points and degrees of freedom in the fitting procedure, respectively.

RESULTS AND DISCUSSION

A488 Is a Good Reporter of Conformational Changes Undergone by Lysozyme. The ability of the covalently conjugated fluorophore A488 to report conformational transitions undergone by the fluorescently labeled enzyme was first tested by performing fluorescence thermal unfolding studies of Lz-A488 at pH 7.4. In fact, thermal denaturation of human and egg-white lysozyme has been extensively studied both experimentally and computationally,[19,45] providing an adequate reference framework to compare our results. Within the 19−55 °C temperature interval, the fluorescence emission intensities of both Lz-A488 and free A488 dye decreased in parallel only 10% (Figure 1a) due to an increase in their nonradiative decay rates with the temperature. Above 60 °C, a cooperative transition with a T_m value of 73.5 °C was recorded only for the fluorescently labeled protein as the enzyme unfolded (Figure 1a). These results agree with the literature, as HEWL secondary and tertiary structures have been described to be highly stable against thermal denaturation in aqueous solution, with very little change between 20 and 64 °C.[45] The unfolding begins with the loss of sheet structures in the lysozyme β-domain and a small part of the helical structures in the α-domain below 70 °C, followed by the concerted unfolding of the tertiary structure at higher temperatures.[45] More detailed information about Lz-A488 could be obtained from time-resolved fluorescence measurements. All the fluorescence intensity decay profiles of Lz-A488 obtained at different temperatures were adequately described by a triexponential function. In principle, the complex fluorescence decay could result from different lysozyme molecules being labeled at distinct sites (ground-state heterogeneity) and/or due to local structural fluctuations of the polypeptide backbone of the native enzyme. At 25 °C, the native Lz-A488 exhibited a nearly monoexponential fluorescence intensity decay with a main lifetime component of 3.6 ns (fractional amplitude ∼0.70). The fractional amplitudes of the short- and intermediate-lived species detected (lifetime components: τ_1 ∼ 0.25 ns and τ_2 ∼ 2 ns) were about 0.07 and 0.24, respectively (Figure 1b). The long and intermediate fluorescence lifetimes of Lz-A488 decreased slightly with the temperature, whereas the short fluorescence lifetime was essentially temperature-independent (Figure 1c). The long-lived fluorescence lifetime was the major component of the intensity decay of Lz-A488 when it retained a natively structured conformation. Upon increasing the temperature above ∼60 °C, the populations of both τ_1 and τ_2 were significantly enhanced until reaching plateau values of 0.36 and 0.38, respectively, at 80 °C (Figure 1b). As a result of both of these changes, the mean fluorescence lifetime, $\langle\tau\rangle_1$, decreased from 3.0 to ∼1.3 ns upon heating the solution from 25 to 90 °C. Altogether, these results are consistent with an additional temperature-dependent quenching mechanism affecting only the conjugated protein above ∼55 °C. This additional quenching can be rationalized in terms of PET from an electron donor present in several possible adjacent amino acid residues (mainly Trp residues) to A488.[33,34] It has been suggested that K97 and K33 are the preferential modification sites of lysozyme, as they exhibit the highest surface accessibility and chemical reactivity.[46−48] Of these residues, K97 is the nearest to the region where temperature-induced lysozyme unfolding starts.[45] Therefore,

dx.doi.org/10.1021/jp310396v | J. Phys. Chem. B 2013, 117, 2906−2917

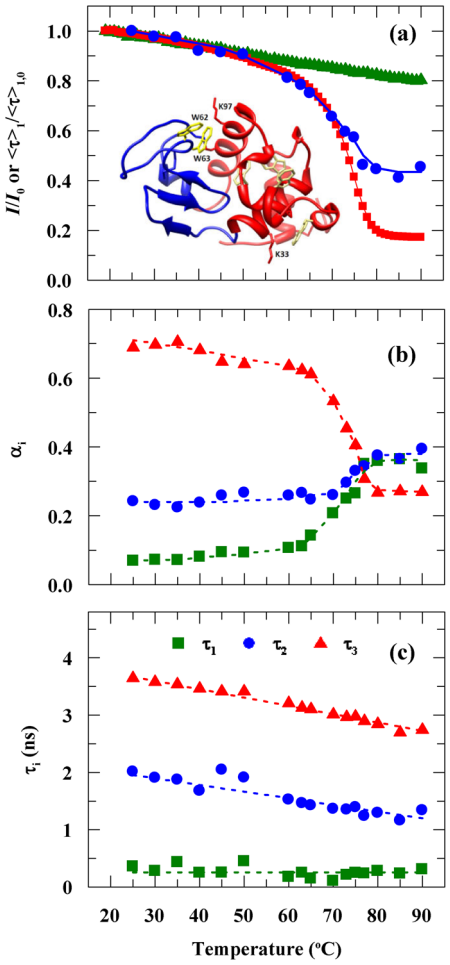

Figure 1. Thermal unfolding of Lz-A488 at pH 7.4 monitored by fluorescence spectroscopy. (a) Temperature dependence of the relative fluorescence intensities, I (Lz-A488, red squares; A488, green triangles), and mean fluorescence lifetimes, $\langle\tau\rangle_1$, (Lz-A488, blue circles) of 1 μM Lz-A488 and free dye. Inset: Representation of HEWL structure showing the location of its most reactive lysine residues: K33 and K97 (PDB ID 4LZT). The α and β domains are shown in red and blue, respectively. Lysozyme's six tryptophan residues (W28, W62, W63, W108, W111, and W123), which are potent electron donors and therefore efficient quenchers, are shown in yellow. Of these residues, W62 and W63 most likely cause temperature-induced changes in quenching of A488 fluorescence because they are present on a long loop in the β domain (within 10 Å distance from K97 in the crystal structure), where lysozyme thermal unfolding begins. The structure was drawn using Chimera.[64] Changes in the (b) pre-exponential factors associated to (c) each lifetime component (i = 1 (green squares), i = 2 (blue circles), and i = 3 (red triangles)) determined from time-resolved fluorescence data for 1 μM Lz-A488 as a function of temperature.

particularly good candidates for temperature-dependent quenchers of A488 fluorescence are residues W62 and W63 located on a long loop in the β domain close to this residue in the native protein (inset of Figure 1a). Upon heating the solution, the increased dynamics of this segment must allow for an increased proximity between W62 and W63 residues and the dye attached to the protein at K97, resulting in an efficient dynamic quenching of its fluorescence by a PET-based mechanism. This is expected to cause an increased population of Lz-A488 molecules, presenting a much shorter excited-state lifetime, as it was observed (Figure 1b). When the quencher and the fluorophore are at van der Waals contact distance, PET becomes extremely efficient, resulting in static quenching (Figure 1a). In conclusion, the quenching of Lz-A488 fluorescence is most likely dominantly reporting local destabilization of the enzyme in its β-domain, which has long been implicated as a site of instability and origin of amyloidogenic behavior.[19,45]

Lysozyme Interaction with Anionic Liposomes Is a Multistage Process That Can Be Tracked by Changes in Lz-A488 Fluorescence Properties. To detect and characterize in detail the intermediate species formed during the interaction of Lz-A488 with anionic phospholipid membranes, both steady-state and time-resolved fluorescence measurements were carried out. Ultimately, we wanted to characterize the putative oligomeric intermediates that might be involved in lysozyme "amyloid-like" fiber formation triggered by its interaction with negatively charged lipid membranes.[11] POPC:POPS 80:20 LUVs were used in most of the studies, and some of the experiments were also performed with LUVs containing 30 mol % POPS. Each sample was prepared independently, and its L/P molar ratio was varied within a wide range in two different ways: (i) either a fixed total Lz-A488 concentration (0.5 or 3.0 μM) was added to different total phospholipid concentrations ($0 < [L]_t < 6$ mM), or (ii) different protein concentrations (0–9 μM) were added to the liposomes at 0.86 mM total phospholipid concentration.

The addition of 3.0 μM Lz-A488 caused a pronounced increase in the 90° light scattered by the lipid suspension as compared to the control (POPC:POPS 80:20 LUVs) (Figure 2a), showing that the fluorescently labeled protein was able to drive the aggregation/fusion of PS-containing liposomes like the unmodified enzyme.[27,31,42] This system exhibits aggregation properties typical of a bridging attraction, namely, the appearance of a maximum in the scattered intensity by the liposome population at ca. 0.4 mM of total lipid concentration. Interestingly, the fluorescence emission spectra of 3.0 μM membrane-bound Lz-A488 presented a 5 nm red-shift with respect to the spectrum obtained in aqueous solution that correlated to the changes in turbidity experienced by the liposome suspensions (Figure 2c). Concomitantly, the fluorescence intensity of Lz-A488 decreased sharply relatively to its value in buffer, reaching a minimum value at ~0.5 mM total phospholipid concentration. Upon further increase of lipid concentration, there was a progressive recovery of this parameter, but still it did not regain its characteristic value in aqueous solution (Figure 2e). A complete different picture was obtained when the protein concentration was decreased 6-fold to 0.5 μM. As shown in Figure 2c, the maximal fluorescence emission peak of 0.5 μM Lz-A488 was found to be independent of the lipid concentration present in solution (λ_{em}^{max} = 516 ± 1 nm), and no protein-mediated aggregation of the lipid vesicles was detected in this case, as the light scattered by the lipid vesicles was identical to the one in the absence of the modified protein (Figure 2a). Furthermore, the fluorescence intensity of the conjugated protein increased only slightly upon varying the lipid concentration from 0 to 6 mM (Figure 2e). The fluorescence properties of Lz-A488 presented the same trend of variation when the second experimental approach was used. Briefly, although the fluorescence intensity of Lz-A488 increased linearly with its concentration in aqueous solution, two linear regimes were detected when the conjugated protein interacted with 0.86 mM POPC:POPS 80:20 LUVs (Figure 2f). The formation of quenched Lz-A488 fluorescent species above

dx.doi.org/10.1021/jp310396v | J. Phys. Chem. B 2013, 117, 2906–2917

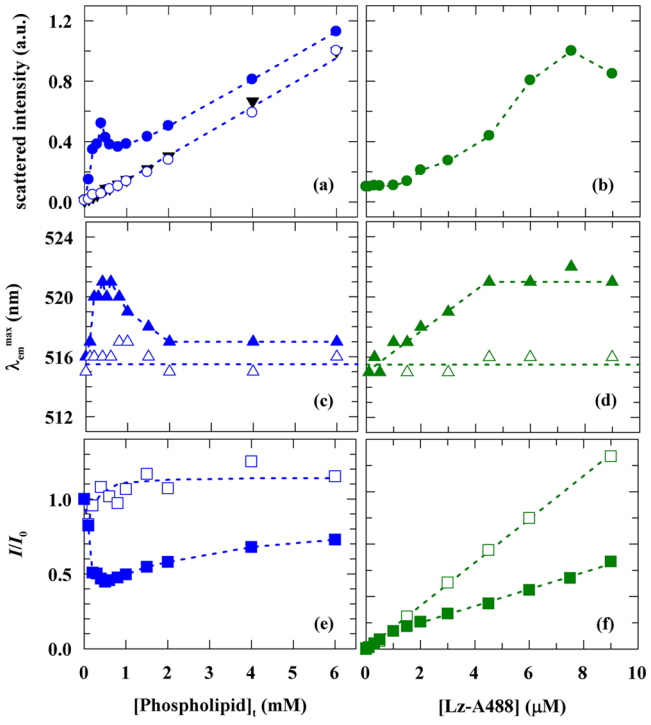

Figure 2. Protein induced aggregation of liposomes and fluorescence changes undergone by Lz-A488 upon membrane partitioning. Changes in (a and b) 90° light scattering of POPC:POPS 80:20 liposomes, (c and d) wavelength of maximum fluorescence intensity, λ_{em}^{max}, and (e and f) relative fluorescence intensities of Lz-A488 as a function of (a, c, and e) total lipid or (b, d, and f) Lz-A488 concentrations (D/P = 0.54). (a, c, and e) [Lz-A488] = 0.5 (open blue symbols) or 3.0 μM (closed blue symbols). (b, d, and f) The measurements were carried out in buffer (open green symbols) or in the presence of 0.86 mM total lipid concentration (closed green symbols). The dotted lines are just a guide to the eye. (a) The closed inverted back triangles are control measurements performed in the absence of protein.

2 μM total protein concentration was again accompanied by a progressive red-shift of its emission spectra from 516 to 521 nm (Figure 2d) and by a sharp increase in the light scattered by the lipid suspension (Figure 2b).

To better characterize the fluorescence changes experienced by Lz-A488 upon varying the L/P ratio of a sample, time-resolved fluorescence measurements were also made. The fluorescence intensity decays of Lz-A488 were always well described by a triexponential function (Supporting Information, Figure S2). The parameters recovered from the fittings (pre-exponential and lifetime components) are presented in Figure 3. Their detailed analysis allows the identification of three consecutive stages in the membrane association of Lz-A488. At stage I, i.e., when the samples were prepared with a high to moderate L/P molar ratio (stage I: $[L]_t$: 6 → 1 mM and [Lz-A488] = 0.5 μM), the Lz-A488 fluorescence intensity decays were essentially indistinguishable from the ones obtained in aqueous solution ($\langle\tau\rangle_1 \sim 3.0$ ns in both cases (Figure 3g and i)). When the L/P molar ratio used in the preparation of the samples was progressively decreased, $\langle\tau\rangle_1$ gradually shortened from 3.0 to ~1.8 ns (stage II: $[L]_t$: 1 → 0.1 mM and [Lz-A488] = 0.5 μM (Figure 3g); $[L]_t$: 6 → 1 mM and [Lz-A488] = 3.0 μM (Figure 3h); $[L]_t$ = 0.86 mM and [Lz-A488]: 0.3 → 3 μM (Figure 3i)). This effect was mostly due to changes in the amplitudes associated to each lifetime component: an increase in the contribution of the short and intermediate decay components (α_1 and α_2, respectively) was accompanied by a concomitant decrease in the amplitude α_3 associated with the longest lifetime component, τ_3, while τ_1 and τ_3 remained essentially invariant and τ_2 decreased from 2 to ~1.3 ns (best illustrated in Figure 3c and f). Finally, stage III was reached when the experiments were performed with even lower L/P molar ratios ($[L]_t$: 1 → 0.1 mM and [Lz-A488] = 3.0 μM (Figure 3h); $[L]_t$ = 0.86 mM and [Lz-A488] > 3 μM (Figure 3i)). Under these conditions, the long-lived lifetime component of the membrane-bound Lz-A488 progressively decreased, reaching a minimum value of ~3.2 ns (Figure 3e and f) and further causing a shortening of the mean fluorescence lifetime of Lz-A488 to ~1.5 ns (Figure 3h and i). It should be noted that this third phase is concomitant to the detection of an extensive protein-mediated liposome aggregation (Figure 2a and b) and is accompanied by a spectral red-shift in Lz-A488 fluorescence emission (Figure 2c and d).

The biphasic behavior presented by the mean fluorescence lifetime of Lz-A488 as a function of total lipid concentration (Figure 3g and h) cannot be explained by a simple partitioning equilibrium of the conjugated protein between the aqueous and lipid phases. We propose that the transition between stages I and II is caused by a shifting of membrane-bound Lz-A488 between two populations of molecules that experience different degrees of quenching due to distinct proximities between the fluorophore and the quencher groups present in the side chains of possible adjacent Trp residues. In other words, as the surface concentration of Lz-A488 increases within the lipid range considered (e.g., $[L]_t$: 6 → 1 mM (Figure 3h) or [Lz-A488]: 0.3 → 3 μM (Figure 3i)), the enzyme progressively adopts a partially unfolded state at the membrane surface. The pronounced surface concentration dependence presented by the mean fluorescence lifetime of Lz-A488 further suggests that the loosening of its packed tertiary structure results in the formation of an aggregation-prone conformer which drives lysozyme oligomerization in the lipid vesicles. The quenching of A488 fluorescence could arise directly from the protein's conformational change (intramolecular PET) or be caused by quaternary interactions through protein−protein interactions (intermolecular PET). The extensive coverage of the liposomes by the positively charged protein is responsible for the final switch from stage II to III. Lysozyme binding to the lipid vesicles decreases the initial strong repulsion between two anionic liposomes, allowing for the juxtaposition of membranes which results in a protein-mediated cross-bridging of the lipid vesicles. This produces a dehydration of the bilayer surface that is accompanied by a lowering of the surface dielectric constant,[29] which results in an increase in hydrophobicity of the bilayer surface, ultimately allowing for a deeper penetration of the protein molecules in the membrane.[49] The protein−lipid interactions at stage III are now predominantly hydrophobic, causing a 5−6 nm red-shift in the membrane-bound Lz-A488 fluorescence emission spectra (Figure 2c and d) and a further decrease of its fluorescence lifetime from 1.8 to ~1.5 ns (Figure 3h and i). Altogether, these results give support to the conclusion that the surface coverage of the lipid vesicles by lysozyme is the major factor governing the photophysical properties of A488 covalently bound to the protein.

Lysozyme Binding to Anionic Lipid Membranes Can Be Globally Analyzed Using a Three-State Model. In order to quantitatively describe the time-resolved fluorescence data obtained for Lz-A488, a two-step model was derived, as detailed in the Materials and Methods (Scheme 1). Briefly, it

dx.doi.org/10.1021/jp310396v | J. Phys. Chem. B 2013, 117, 2906−2917

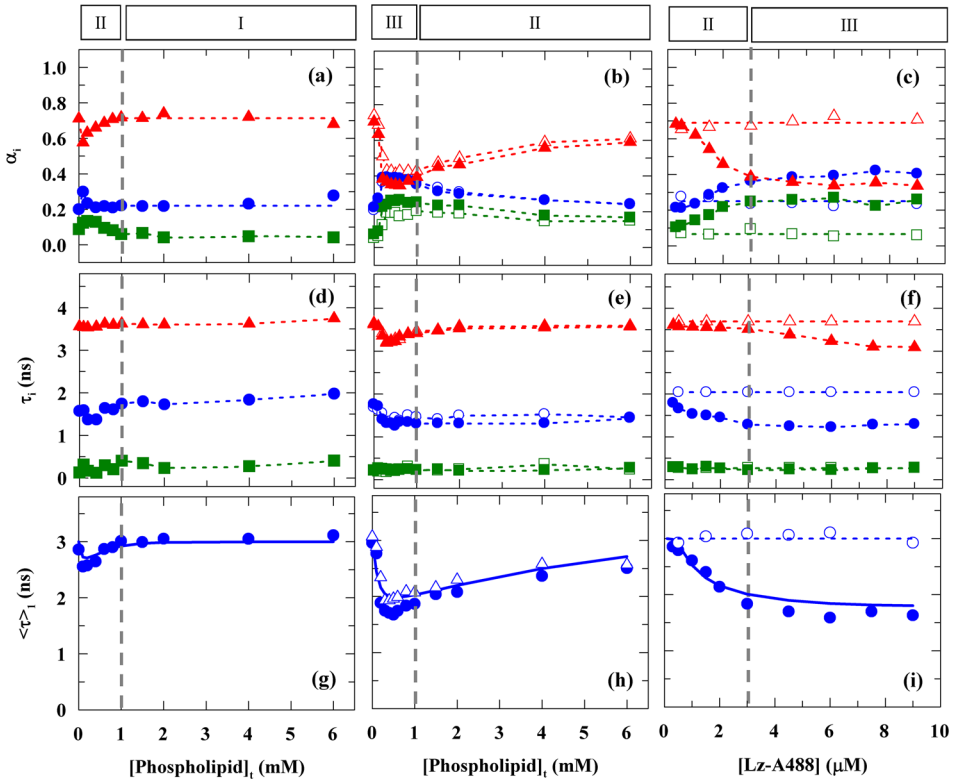

Figure 3. Changes of time-resolved fluorescence parameters of Lz-A488 upon membrane partitioning. (a, b, c) The amplitudes, α_i, of (d, e, f) lifetime components, τ_i (i = 1 (squares), i = 2 (circles), and i = 3 (triangles)) and (g, h, i) the mean fluorescence lifetimes, $\langle\tau\rangle_1$, from Lz-A488 were measured in the presence of increasing concentrations of POPC:POPS 80:20 LUVs (left and central panels) or Lz-A488 (right panels). The protein concentrations used in the left and central panels were 0.5 (D/P = 0.54) and 3.0 μM (D/P = 0.30 (open symbols); D/P = 0.54 (closed symbols)), respectively. In the right panels, the fluorescence intensity decays of Lz-A488 (D/P = 0.54) were measured in buffer (open symbols) or in the presence of 0.86 mM total lipid (closed symbols). The gray vertical dashed lines indicate the boundaries between stages I, II, and III identified in the text. The solid blue curves of the bottom panels are the global best-fit of the cooperative partition model including electrostatic effects presented in the Materials and Methods section to the mean fluorescence lifetime data (k = 6 and $K_{ag} = 2 \times 10^{14}$ (n = 71)). The dashed vertical lines are just a guide to the eye.

was assumed that (i) monomeric lysozyme binds to the bilayer surface according to a simple partitioning equilibrium governed by a partition coefficient previously determined by FCS measurements[26] and (ii) reversibly assembles into oligomers with k subunits. Furthermore, it was considered that k-meric assemblies of lysozyme present a much shorter fluorescence lifetime ($\langle\tau\rangle_1^{mk}$ = 1.5 ns) than the free or membrane-bound monomeric Lz-A488 (i.e., $\langle\tau\rangle_1^{w1} = \langle\tau\rangle_1^{m1}$ = 3.0 ns). For simplification, stages II and III described above were merged in this analysis because the last step exerted only a minor influence on the fluorescence decay kinetics presented by membrane-bound Lz-A488. Additionally, the gradual decrease of lysozyme membrane partition coefficient due to partial neutralization of the surface potential of the liposomes was also taken into account explicitly in this model using the Gouy−Chapman theory.[38]

The three-state cooperative partition model was globally fitted to the experimentally measured $\langle\tau\rangle_1$ as a function of total phospholipid or Lz-A488 concentrations. The fitting was performed in a two-step iterative procedure: after first optimizing the effective lysozyme charge to z_p = 3.5, the sum of squared residuals (eq 10) was minimized by varying the aggregation constant, K_{ag}, while k was kept fixed at different integer values. Figure 4 shows that lysozyme reversibly assembles into aggregates of $k \geq 6$ molecules when interacting with POPC LUVs containing 20 or 30 mol % POPS. The high

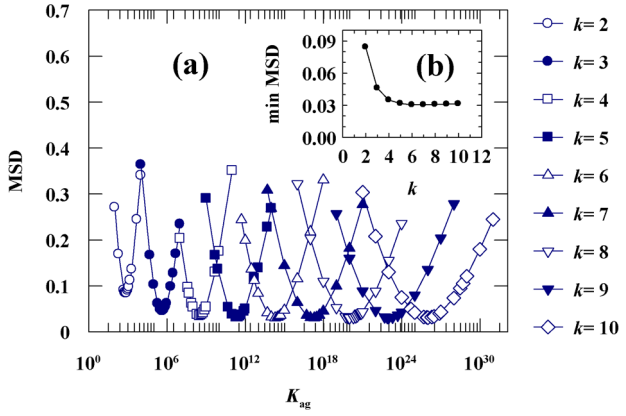

Figure 4. (a) Dependence of the mean-square deviation (MSD) with the aggregation constant, K_{ag}, obtained during the fitting of the three-state cooperative partition model including electrostatic effects to the mean fluorescence lifetimes of Lz-A488. (a) K_{ag} was allowed to vary in each fit while k, the oligomerization number of Lz-A488 on the membrane, was kept constant at different integer numbers. (b) The minimum of each parabola is plotted as a function of k.

correlation between k and K_{ag} prevents further improvement on the characterization of the oligomerization state of lysozyme in the membranes at this point. In fact, these two parameters can be related using

dx.doi.org/10.1021/jp310396v | J. Phys. Chem. B 2013, 117, 2906−2917

$$K_a^{(k-1)} = \frac{\frac{[Lz_m^k]}{[L]_{ac}}}{\left(\frac{[Lz_m^1]}{[L]_{ac}}\right)^k} \quad (11)$$

where K_a is the intrinsic surface aggregation constant of lysozyme related to the stepwise addition of a protein monomer to the aggregate ($(k-1)$-mer). In our system (POPC LUVs containing variable mol % POPS), $K_a = 734 \pm 38$ for $k \geq 6$. Figure 3g, h, and i and Figure S3 in the Supporting Information illustrate the fitting of the three-state model to the experimental data using $k = 6$ as an example ($n = 71$). The global fitting was quite good considering that the data was obtained in six independent experiments employing very different experimental conditions: two different mol % POPS (20 and 30 mol %), two orthogonal experimental designs (keeping the protein concentration fixed and varying the phospholipid concentration and vice versa), and three different protein batches prepared with variable D/P.

The value obtained for the effective charge ($z_p = +3.5$) is considerably less than the one expected for lysozyme net charge at pH 7.4 ($z = +8$).[27] This is in agreement with other binding studies of peripheral proteins and peptides to membranes[50−53] and is probably related to the nonuniform charge distribution of the protein/peptide; i.e., the protein charge exposed to the membrane surface might not be equal to the formal net charge of the protein/peptide. In addition, labeling lysozyme with A488 is expected to decrease the protein's net charge by +3.[54] Another factor that might also contribute to the difference registered between the two values is that, due to its large size, the charge of the protein is distributed along a spatial dimension of about the same size as the thickness of the electric double layer. Other assumptions were also made in the derivation of the cooperative model used in this work that warrant further discussion. First, a discrete oligomerization model, rather than a nucleation−elongation model, was used to describe lysozyme oligomerization in the lipid vesicles.[55] Although this is a simple two-state model that neglects the formation of intermediate aggregates of variable sizes, it requires less fitting parameters than the second more general protein aggregation model. The first approach was therefore used here because the number of free parameters involved in fitting the cooperative partition model combined with the Gouy−Chapman theory to the lifetime data of Lz-A488 is already very large. Second, the liposome interfacial area was assumed to be invariant, ignoring that some disturbance of the lipid surface must occur due to partial lysozyme insertion in the lipid vesicles upon its oligomerization. An increased accessibility of phospholipid to the protein due to multilayer formation might also contribute to increase the maximum lysozyme binding capacity of the liposomes at stage III. Finally, area exclusion effects at high membrane occupancy were not considered in our model.[56,57] These are known to become significant above a membrane surface coverage of 10%, i.e., at high degrees of binding.[58] Simple geometrical calculations allowed us to conclude that these effects are more important when stage III is reached in our system.

Although qualitatively similar conclusions were obtained earlier by other investigators regarding lysozyme oligomerization upon its interaction with negatively charged lipid bilayers,[48,59] there are important differences between our work relative to these previous studies that should be stressed. First, the present experimental design is more rigorous, as a much wider range of total phospholipid/protein concentrations was explored in this study, allowing us to test our three-state cooperative partition model combined with the Gouy−Chapman theory under a more vast set of experimental conditions. Second, our results are much more informative as compared to the steady-state study of Gorbenko et al.,[48] because the use of time-resolved fluorescence measurements proved to be crucial in the identification and spectroscopic characterization of distinct membrane-bound fluorescently labeled lysozyme species as a function of the surface coverage of the liposomes. This allowed us to clearly identify three consecutive lysozyme membrane-interaction stages. Third, lysozyme partition coefficients were not a fitting parameter in our model, since they had been previously determined experimentally for Lz-A488 using FCS.[26] This allowed for a much more stringent global analysis of the experimental binding curves obtained in this study that nevertheless were still successfully described using a single self-consistent set of parameters (aggregation constant and stoichiometry) at variance with the study of Gorbenko et al.[48] Finally, in the recent Förster resonance energy transfer work of Trusova et al.,[59] one of the acceptor labels used was covalently attached to a lysozyme cysteine residue after reducing the protein disulfide bonds with dithiotreitol. This experimental procedure most probably caused lysozyme misfolding before its interaction with the anionic lipid vesicles, hampering the conclusions obtained in their study.

The Cooperative Partition Model Combined with the Gouy−Chapman Theory Explains the Biphasic Changes of Membrane-Bound Lz-A488 Fluorescence Properties. It is also relevant to compare how the protein partition coefficient and the fractional populations of each lysozyme species vary with the experimental conditions employed. Figure 5 exemplifies the results obtained using the best fitting parameter set found for $k = 6$. This allows showing that the biphasic behavior presented by the fluorescence properties of Lz-A488 in some experiments of this study results from a delicate balance between the long-range electrostatic effects involved in lysozyme partitioning to the negatively charged membranes and its oligomerization in the lipid vesicles. According to a simple partition equilibrium, the surface concentration of lysozyme in the liposomes is expected to increase either by gradually reducing the total phospholipid concentration in solution when a fixed protein concentration is used or by adding increasing amounts of the protein to a constant phospholipid concentration. At some point in this process, a high enough lysozyme membrane surface concentration is reached, triggering its oligomerization. For $k = 6$, our model predicts that the onset for lysozyme oligomerization occurs at a molar ratio of $[Lz_m^1]/[L_{ac}] \sim 0.0009$ (Supporting Information, Figure S4) which corresponds to a fractional coverage of the lipid bilayer−water interface by monomeric membrane-bound lysozyme molecules of ca. 2%. Above this concentration threshold, a cooperative partition of lysozyme to the membranes is established; i.e., the growth of the oligomer population in the liposomes is made at the expense of a progressive recruitment of more lysozyme monomers from the aqueous solution to the membrane, since the two equilibria (lysozyme partition and self-association) are coupled. This effect can be quantitatively described by calculating an effective partition coefficient, K_p^{effec}, for lysozyme that takes into account the k-mers in addition to the lysozyme monomers present in the membrane:

dx.doi.org/10.1021/jp310396v | J. Phys. Chem. B 2013, 117, 2906−2917

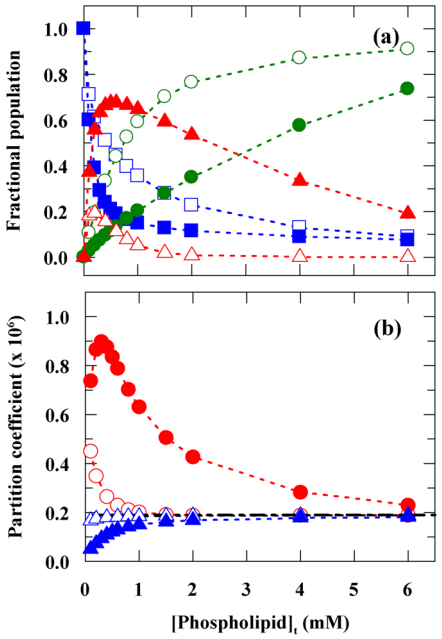

Figure 5. Cooperative partition model including electrostatic effects describing lysozyme interaction with POPC LUVs containing 20 mol % POPS. Variation of (a) the fractional populations and (b) partition coefficients of Lz-A488 with the total phospholipid concentration. (a) The fractions of aqueous and membrane-bound monomeric and hexameric lysozyme species (squares, circles, and triangles, respectively) were calculated using $k = 6$ and $K_{ag} = 2 \times 10^{14}$ ($z_p = 3.5$). (b) The partition coefficient of Lz-A488 determined by FCS, K_p^{FCS}, is depicted by a dashed horizontal line, K_p^{cor} (blue triangles) is the partition coefficient corrected for the screening of the interfacial membrane charge according to the Gouy–Chapman theory, and K_p^{effec} (red circles) takes into account the k-mers in addition to monomeric Lz-A488 present in the lipid bilayer. [Lz-A488] = 0.5 (open symbols) or 3.0 μM (closed symbols).

$$K_p^{effec} = \frac{\frac{([Lz_m^1] + k[Lz_m^k])}{[L]_{ac}}}{\frac{[Lz_w^1]}{[W]}} \quad (12)$$

Figure 5b shows that this parameter can reach a value that is almost 5-fold higher than the partition coefficient determined for Lz-A488 using FCS. On the other hand, the partition coefficient of lysozyme corrected for electrostatic effects, K_p^{cor}, steadily decreases when a fixed protein concentration is used and the total phospholipid concentration in solution is gradually reduced from 6 to 0.1 mM. As lysozyme oligomerization proceeds in the membrane, this effect becomes even more pronounced (Figure 5b). Eventually, the reduction of lysozyme partition coefficient due to the shielding of the membrane surface potential is so important that Lz-A488 surface concentration in the membranes starts to decrease instead of augment. The extension of lysozyme oligomerization in the membranes is then reduced, which, in turn, causes an increase in Lz-A488 fluorescence intensity/mean fluorescence lifetime because less quenched lysozyme fluorescent species (oligomers) are produced. Finally, it should be stressed that under none of the experimental conditions used in this study (use of a low ionic strength buffer and a moderate acidic phospholipid content) lysozyme partitioned into membranes so strongly that it was completely membrane-bound. In other words, there was always a significant, although variable, molar fraction of aqueous lysozyme in all the samples studied (Figure 5a).

Lz-A488 Is Predominantly Oligomerized in the Lipid–Protein Supramolecular Complexes (Fibers) Formed at a Low L/P Ratio as Revealed by FLIM Measurements. Finally, FLIM measurements were used to check whether the dominant Lz-A488 species present in the "amyloid-like" fibers formed upon lysozyme interaction with liposomes containing anionic phospholipids at a low L/P ratio was monomeric or oligomeric. These supramolecular lipid–protein mixed assemblies were prepared according to the protocol described by Kinnunen and co-workers,[11,60] and CLSM was used to image the samples. They were found to be morphologically heterogeneous, with fiber-like structures coexisting with other amorphous aggregates. Sample imaging further showed that Lz-A488 (Figure 6a) and a fluorescently labeled phospholipid (Figure 6b) were both incorporated into the long and thick micrometer-sized mesoscopic entities that presented morphological features consistent with fibers. These must correspond to the multilamellar structures proposed earlier to be formed in solution upon lysozyme interaction with negatively charged membranes.[42] The fluorescence decay kinetics of Lz-A488 embedded in these fibers was then measured by FLIM (see the Supporting Information). As exemplified in Figure 6c, the mean fluorescence lifetime of Lz-A488 had a relatively uniform spatial distribution in these fibers (the color of each pixel in the image corresponds to a different mean fluorescence lifetime value). The histogram of mean fluorescence lifetimes was rather narrow and centered around 1.4 ns, a value close to the one measured for Lz-A488 in stage III of lysozyme interaction with anionic liposomes (bulk measurements). Therefore, we conclude that this fluorescently labeled protein is predominantly assembled into quenched oligomers in these fibers. Recently, it was shown that exposing a culture of human neuroblastoma SHSY-5Y to these lipid–protein complexes incubated for several days resulted in cell viability impairment.[32]

CONCLUSIONS

This study aimed to detect and characterize the lipid-induced intermediates present along the aggregation pathway of lysozyme in an anionic membrane environment that putatively leads to the formation of "amyloid-like" fibers at a low L/P ratio.[11] In particular, we wanted to elucidate in detail how progressive variations in the membrane surface charge density/crowding and protein-mediated vesicle clustering modulated the membrane-induced structural rearrangements and oligomerization of lysozyme in interaction with anionic liposomes. This issue was addressed here by covalently linking to the lysozyme molecule a PET-sensitive fluorescent probe, A488, and complementary insights were obtained by performing time-resolved fluorescence intensity measurements at both the ensemble average (bulk) and single-fiber level. Lysozyme interaction with anionic liposomes was found to be a complex multistage process that critically depended on the protein coverage of the liposomes in agreement with previous studies carried out with other basic/peripheral binding proteins.[61−63] As the L/P molar ratio of each sample was varied, our bulk time-resolved fluorescence data allowed tracking in detail the consecutive formation of three well differentiated membrane-bound Lz-A488 populations that presented distinct spectroscopic signatures. At a high L/P molar ratio (stage I), electrostatically driven superficial membrane binding of Lz-

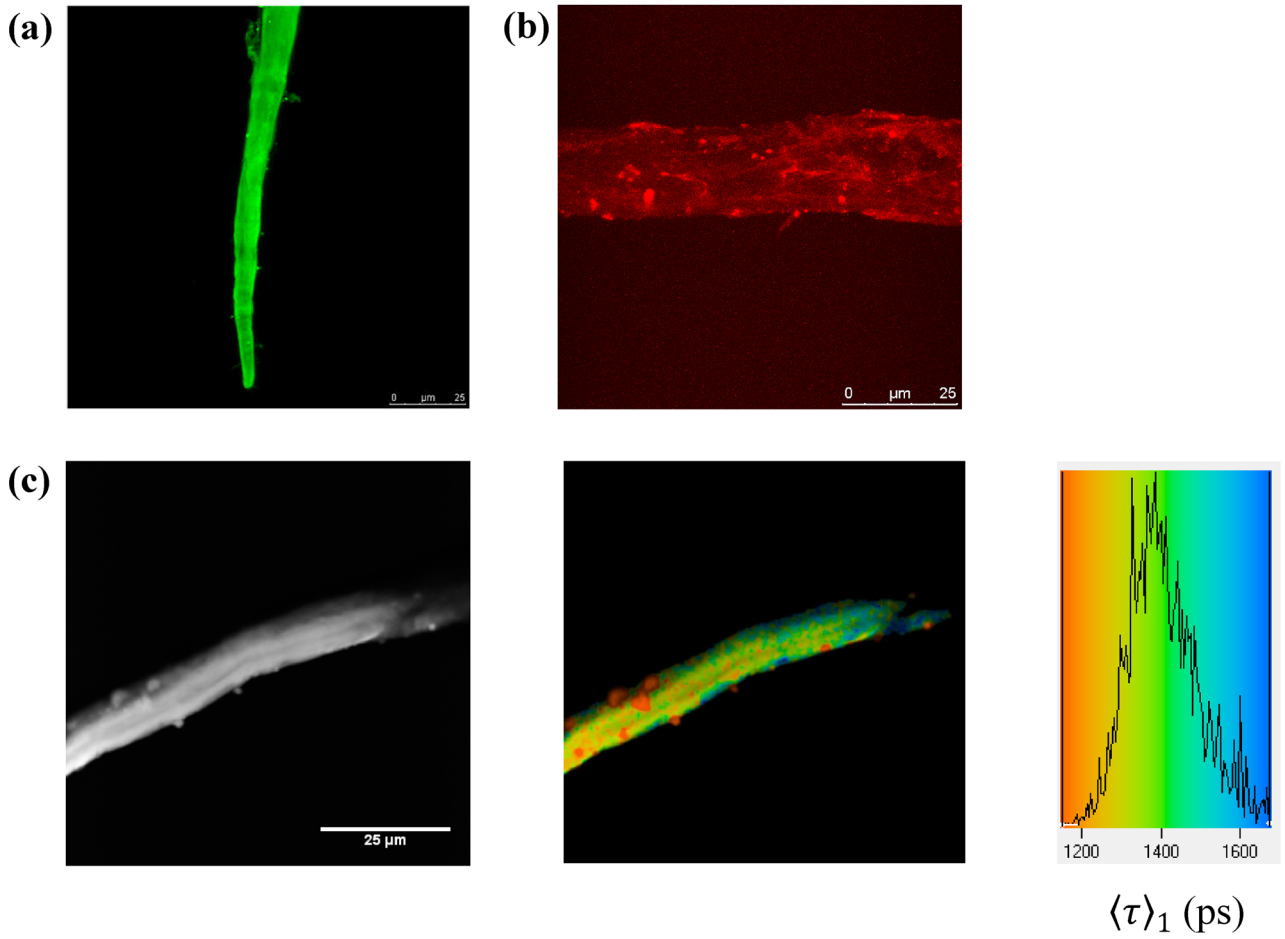

Figure 6. Characterization of lipid−protein fibers formed at a low L/P ratio by (a and b) CLSM and (c) FLIM. CLSM images of the fibers prepared with (a) Lz-A488 or (b) Rhod-DOPE-doped LUVs. (c) Two-photon excitation fluorescence intensity image (left panel), fluorescence lifetime (FLIM) image (middle panel), and fluorescence lifetime distribution histogram of the respective FLIM image (right panel) of these structures that present a mean fluorescence lifetime around 1.4 ns.

A488 at "infinite surface dilution" dominates. Under these conditions, the membrane-bound conjugated protein retains an essentially native-like fold, as its fluorescence emission properties are identical to the ones presented in solution (λ_{em}^{max} = 516 ± 1 nm and $\langle\tau\rangle_1$ = 3.0 ns). When moderate L/P molar ratios are used (stage II), a more pronounced neutralization of the liposome's surface charge by the protein causes a partial unfolding of the membrane-bound Lz-A488 that is coupled to increased formation of multimeric species. These species characteristically present a more quenched mean fluorescence lifetime than the free Lz-A488 ($\langle\tau\rangle_1 \sim$ 1.8 ns). Finally, at very low L/P molar ratios (stage III), the 5−6 nm red-shift detected in Lz-A488 fluorescence emission spectra and a further reduction of its mean fluorescence lifetime to ∼1.5 ns report a switching in the lysozyme membrane binding mode from a peripheral binding to a partial insertion into the hydrophobic core of the membrane. Most importantly, these spectroscopic alterations were accompanied by an increase in the turbidity of the liposome suspension due to an extensive protein-mediated cross-bridging of the anionic lipid vesicles. Elongated structures appeared in solution that were confirmed by CLSM to contain the fluorescently labeled protein and lipid. Furthermore, FLIM images of these fibers prepared with Lz-A488 at a low L/P ratio revealed quite homogeneous profiles centered at around 1.4 ns. This quenched mean fluorescence lifetime indicates that Lz-A488 is predominantly assembled into oligomers when embedded in these fibers.

A three-state cooperative partition model combined with the Gouy−Chapman theory was globally fitted to several Lz-A488 membrane binding curves (variation of the mean fluorescence lifetime of Lz-A488 as a function of a wide range of total phospholipid/protein concentrations) measured at the ensemble average level. A single set of parameters (K_a = 734 ± 38 for $k \geq 6$ and z_p = +3.5) was able to consistently describe the mean fluorescence lifetime data obtained using two orthogonal experimental designs and liposomes prepared with a variable anionic phospholipid content (20 and 30 mol % POPS). In summary, our study provides important information about the alterations undergone at the tertiary and quaternary levels by lysozyme, a basic protein, in interaction with anionic POPC:POPS liposomes, and the manner in which these changes are coupled to the structural alterations experienced by the lipid vesicles in its presence. Our results underlie the importance of new stabilizing interactions with the anionic lipids in defining the conformational properties of membrane-bound Lz-A488 and clearly show that its binding to negatively charged membranes results in cooperative events, i.e., formation of k-mers with $k \geq 6$.

dx.doi.org/10.1021/jp310396v | J. Phys. Chem. B 2013, 117, 2906−2917

■ ASSOCIATED CONTENT

Supporting Information

Additional methods and four figures. This material is available free of charge via the Internet at http://pubs.acs.org.

■ AUTHOR INFORMATION

Corresponding Author

*E-mail: ana.coutinho@ist.utl.pt. Phone: +351 218419248. Fax: +351 218464455.

Notes

The authors declare no competing financial interest.

■ ACKNOWLEDGMENTS

The authors acknowledge Fundação para a Ciência e Tecnologia (Project PTDC/QUI-BIQ/099947/2008 and Ph.D. grant SFRH/BD/61723/2009 to A.M.M.) for financial support.

■ REFERENCES

(1) Chiti, F.; Dobson, C. M. Protein Misfolding, Functional Amyloid, and Human Disease. *Annu. Rev. Biochem.* **2006**, *75*, 333−366.

(2) Eisenberg, D.; Jucker, M. The Amyloid State of Proteins in Human Diseases. *Cell* **2012**, *148*, 1188−1203.

(3) Guijarro, J. I.; Sunde, M.; Jones, J. A.; Campbell, I. D.; Dobson, C. M. Amyloid Fibril Formation by an SH3 Domain. *Proc. Natl. Acad. Sci. U.S.A.* **1998**, *95*, 4224−4228.

(4) Chiti, F.; Webster, P.; Taddei, N.; Clark, A.; Stefani, M.; Ramponi, G.; Dobson, C. M. Designing Conditions for in Vitro Formation of Amyloid Protofilaments and Fibrils. *Proc. Natl. Acad. Sci. U.S.A.* **1999**, *96*, 3590−3594.

(5) Stefani, M.; Dobson, C. M. Protein Aggregation and Aggregate Toxicity: New Insights Into Protein Folding, Misfolding Diseases and Biological Evolution. *J. Mol. Med.* **2003**, *81*, 678−699.

(6) Gorbenko, G. P.; Kinnunen, P. K. J. The Role of Lipid-Protein Interactions in Amyloid-Type Protein Fibril Formation. *Chem. Phys. Lipids* **2006**, *141*, 72−82.

(7) Aisenbrey, C.; Borowik, T.; Bystrom, R.; Bokvist, M.; Lindstrom, F.; Misiak, H.; Sani, M. A.; Grobner, G. How Is Protein Aggregation in Amyloidogenic Diseases Modulated by Biological Membranes? *Eur. Biophys. J. Biophys. Lett.* **2008**, *37*, 247−255.

(8) Hebda, J. A.; Miranker, A. D. The Interplay of Catalysis and Toxicity by Amyloid Intermediates on Lipid Bilayers: Insights from Type II Diabetes. *Ann. Rev. Biophys.* **2009**, *38*, 125−152.

(9) Kayed, R.; Head, E.; Thompson, J. L.; McIntire, T. M.; Milton, S. C.; Cotman, C. W.; Glabe, C. G. Common Structure of Soluble Amyloid Oligomers Implies Common Mechanism of Pathogenesis. *Science* **2003**, *300*, 486−489.

(10) Williams, T. L.; Serpell, L. C. Membrane and Surface Interactions of Alzheimer's Aβ Peptide - Insights Into the Mechanism of Cytotoxicity. *FEBS J.* **2011**, *278*, 3905−3917.

(11) Zhao, H. X.; Tuominen, E. K. J.; Kinnunen, P. K. J. Formation of Amyloid Fibers Triggered by Phosphatidylserine-Containing Membranes. *Biochemistry* **2004**, *43*, 10302−10307.

(12) Zhao, H. X.; Jutila, A.; Nurminen, T.; Wickstrom, S. A.; Keski-Oja, J.; Kinnunen, P. K. J. Binding of Endostatin to Phosphatidylserine-Containing Membranes and Formation of Amyloid-Like Fibers. *Biochemistry* **2005**, *44*, 2857−2863.

(13) Zhao, H.; Sood, R.; Jutila, A.; Bose, S.; Fimland, G.; Nissen-Meyer, J.; Kinnunen, P. K. J. Interaction of the Antimicrobial Peptide Pheromone Plantaricin A with Model Membranes: Implications for a Novel Mechanism of Action. *Biochim. Biophys. Acta* **2006**, *1758*, 1461−1474.

(14) Domanov, Y. A.; Kinnunen, P. K. J. Antimicrobial Peptides Temporins B and L Induce Formation of Tubular Lipid Protrusions from Supported Phospholipid Bilayers. *Biophys. J.* **2006**, *91*, 4427−4439.

(15) Sood, R.; Domanov, Y.; Kinnunen, P. K. J. Fluorescent Temporin B Derivative and Its Binding to Liposomes. *J. Fluoresc.* **2007**, *17*, 223−234.

(16) Sood, R.; Domanov, Y.; Pietiainen, M.; Kontinen, V. P.; Kinnunen, P. K. J. Binding of LL-37 to Model Biomembranes: Insight Into Target Vs Host Cell Recognition. *Biochim. Biophys. Acta* **2008**, *1778*, 983−996.

(17) Code, C.; Domanov, Y.; Jutila, A.; Kinnunen, P. K. J. Amyloid-Type Fiber Formation in Control of Enzyme Action: Interfacial Activation of Phospholipase A(2). *Biophys. J.* **2008**, *95*, 215−224.

(18) Code, C.; Domanov, Y. A.; Killian, J. A.; Kinnunen, P. K. J. Activation of Phospholipase A(2) by Temporin B: Formation of Antimicrobial Peptide-Enzyme Amyloid-Type Cofibrils. *Biochim. Biophys. Acta* **2009**, *1788*, 1064−1072.

(19) Trexler, A. J.; Nilsson, M. R. The Formation of Amyloid Fibrils from Proteins in the Lysozyme Family. *Curr. Protein Pept. Sci.* **2007**, *8*, 537−557.

(20) Pepys, M. B.; Hawkins, P. N.; Booth, D. R.; Vigushin, D. M.; Tennent, G. A.; Soutar, A. K.; Totty, N.; Nguyen, O.; Blake, C. C. F.; Terry, C. J.; et al. Human Lysozyme Gene Mutations Cause Hereditary Systemic Amyloidosis. *Nature* **1993**, *362*, 553−557.

(21) Booth, D. R.; Sunde, M.; Bellotti, V.; Robinson, C. V.; Hutchinson, W. L.; Fraser, P. E.; Hawkins, P. N.; Dobson, C. M.; Radford, S. E.; Blake, C. C. F.; et al. Instability, Unfolding and Aggregation of Human Lysozyme Variants Underlying Amyloid Fibrillogenesis. *Nature* **1997**, *385*, 787−793.

(22) Ibrahim, H. R.; Thomas, U.; Pellegrini, A. A Helix-Loop-Helix Peptide at the Upper Lip of the Active Site Cleft of Lysozyme Confers Potent Antimicrobial Activity with Membrane Permeabilization Action. *J. Biol. Chem.* **2001**, *276*, 43767−43774.

(23) Ibrahim, H. R.; Higashiguchi, S.; Koketsu, M.; Juneja, L. R.; Kim, M.; Yamamoto, T.; Sugimoto, Y.; Aoki, T. Partially Unfolded Lysozyme at Neutral pH Agglutinates and Kills Gram-Negative and Gram-Positive Bacteria Through Membrane Damage Mechanism. *J. Agric. Food Chem.* **1996**, *44*, 3799−3806.

(24) Ibrahim, H. R.; Matsuzaki, T.; Aoki, T. Genetic Evidence that Antibacterial Activity of Lysozyme Is Independent of Its Catalytic Function. *FEBS Lett.* **2001**, *506*, 27−32.

(25) Nash, J. A.; Ballard, T. N. S.; Weaver, T. E.; Akinbi, H. T. The Peptidoglycan-Degrading Property of Lysozyme Is Not Required for Bactericidal Activity in Vivo. *J. Immunol.* **2006**, *177*, 519−526.

(26) Melo, A. M.; Prieto, M.; Coutinho, A. The Effect of Variable Liposome Brightness on Quantifying Lipid-Protein Interactions Using Fluorescence Correlation Spectroscopy. *Biochim. Biophys. Acta* **2011**, *1808*, 2559−2568.

(27) Bergers, J. J.; Vingerhoeds, M. H.; Vanbloois, L.; Herron, J. N.; Janssen, L. H. M.; Fischer, M. J. E.; Crommelin, D. J. A. The Role of Protein Charge in Protein-Lipid Interactions. pH-Dependent Changes of the Electrophoretic Mobility of Liposomes Through Adsorption of Water-Soluble, Globular Proteins. *Biochemistry* **1993**, *32*, 4641−4649.

(28) Pap, E. H. W.; Houbiers, M. C.; Santema, J. S.; vanHoek, A.; Visser, A. Quantitative Fluorescence Analysis of the Adsorption of Lysozyme to Phospholipid Vesicles. *Eur. Biophys. J. Biophys. Lett.* **1996**, *24*, 223−231.

(29) Zschornig, O.; Paasche, G.; Thieme, C.; Korb, N.; Fahrwald, A.; Arnold, K. Association of Lysozyme with Phospholipid Vesicles Is Accompanied by Membrane Surface Dehydration. *Gen. Physiol. Biophys.* **2000**, *19*, 85−101.

(30) Zschornig, O.; Paasche, G.; Thieme, C.; Korb, N.; Arnold, K. Modulation of Lysozyme Charge Influences Interaction with Phospholipid Vesicles. *Colloids Surf., B* **2005**, *42*, 69−78.

(31) Al Kayal, T.; Nappini, S.; Russo, E.; Berti, D.; Bucciantini, M.; Stefani, M.; Baglioni, P. Lysozyme Interaction with Negatively Charged Lipid Bilayers: Protein Aggregation and Membrane Fusion. *Soft Matter* **2012**, *8*, 4524−4534.

(32) Al Kayal, T.; Russo, E.; Pieri, L.; Caminati, G.; Berti, D.; Bucciantini, M.; Stefani, M.; Baglioni, P. Interactions of Lysozyme with Phospholipid Vesicles: Effects of Vesicle Biophysical Features on Protein Misfolding and Aggregation. *Soft Matter* **2012**, *8*, 9115−9126.

(33) Doose, S.; Neuweiler, H.; Sauer, M. Fluorescence Quenching by Photoinduced Electron Transfer: A Reporter for Conformational Dynamics of Macromolecules. *ChemPhysChem* **2009**, *10*, 1389−1398.
(34) Chen, H. M.; Ahsan, S. S.; Santiago-Berrios, M. B.; Abruna, H. D.; Webb, W. W. Mechanisms of Quenching of Alexa Fluorophores by Natural Amino Acids. *J. Am. Chem. Soc.* **2010**, *132*, 7244−7245.
(35) Choi, J.; Kim, S.; Tachikawa, T.; Fujitsuka, M.; Majima, T. Unfolding Dynamics of Cytochrome c Revealed by Single-Molecule and Ensemble-Averaged Spectroscopy. *Phys. Chem. Chem. Phys.* **2011**, *13*, 5651−5658.
(36) Rapson, A. C.; Hossain, M. A.; Wade, J. D.; Nice, E. C.; Smith, T. A.; Clayton, A. H. A.; Gee, M. L. Structural Dynamics of a Lytic Peptide Interacting with a Supported Lipid Bilayer. *Biophys. J.* **2011**, *100*, 1353−1361.
(37) Lindhoud, S.; Westphal, A. H.; Visser, A.; Borst, J. W.; van Mierlo, C. P. M. Fluorescence of Alexa Fluor Dye Tracks Protein Folding. *PLoS One* **2012**, *7*, e46838.
(38) McLaughlin, S. The Electrostatic Properties of Membranes. *Annu. Rev. Biophys. Biophys. Chem.* **1989**, *18*, 113−136.
(39) Haugland, R. P. *The Handbook. A Guide to Fluorescent Probes and Labeling Technologies*, 10th ed., Eugene, OR, 2005.
(40) Pace, C. N.; Vajdos, F.; Fee, L.; Grimsley, G.; Gray, T. How to Measure and Predict the Molar Absorption Coefficient of a Protein. *Protein Sci.* **1995**, *4*, 2411−2423.
(41) McClare, C. W. F. An Accurate and Convenient Organic Phosphorus Assay. *Anal. Biochem.* **1971**, *39*, 527−530.
(42) Coutinho, A.; Loura, L. M. S.; Fedorov, A.; Prieto, M. Pinched Multilamellar Structure of Aggregates of Lysozyme and Phosphatidylserine-Containing Membranes Revealed by FRET. *Biophys. J.* **2008**, *95*, 4726−4736.
(43) White, S. H.; Wimley, W. C.; Ladokhin, A. S.; Hristova, K. Protein Folding in Membranes: Determining Energetics of Peptide-Bilayer Interactions. *Methods Enzymol.* **1998**, *295*, 62−87.
(44) Lantzsch, G.; Binder, H.; Heerklotz, H.; Wendling, M.; Klose, G. Surface Areas and Packing Constraints in POPC/C(12)EO(n) Membranes. A Time-Resolved Fluorescence Study. *Biophys. Chem.* **1996**, *58*, 289−302.
(45) Meersman, F.; Atilgan, C.; Miles, A. J.; Bader, R.; Shang, W. F.; Matagne, A.; Wallace, B. A.; Koch, M. H. J. Consistent Picture of the Reversible Thermal Unfolding of Hen Egg-White Lysozyme from Experiment and Molecular Dynamics. *Biophys. J.* **2010**, *99*, 2255−2263.
(46) Suckau, D.; Mak, M.; Przybylski, M. Protein Surface Topology-Probing by Selective Chemical Modification and Mass Spectrometric Peptide Mapping. *Proc. Natl. Acad. Sci. U.S.A.* **1992**, *89*, 5630−5634.
(47) Teske, C. A.; Simon, R.; Niebisch, A.; Hubbuch, J. Changes in Retention Behavior of Fluorescently Labeled Proteins During Ion-Exchange Chromatography Caused by Different Protein Surface Labeling Positions. *Biotechnol. Bioeng.* **2007**, *98*, 193−200.
(48) Gorbenko, G. P.; Ioffe, V. M.; Kinnunen, P. K. J. Binding of Lysozyme to Phospholipid Bilayers: Evidence for Protein Aggregation Upon Membrane Association. *Biophys. J.* **2007**, *93*, 140−153.
(49) Yuan, B.; Xing, L. L.; Zhang, Y. D.; Lu, Y.; Luo, Y. Y.; Mai, Z. H.; Li, M. Penetration and Saturation of Lysozyme in Phospholipid Bilayers. *J. Phys. Chem. B* **2007**, *111*, 6151−6155.
(50) Heimburg, T.; Marsh, D. Protein Surface-Distribution and Protein-Protein Interactions in the Binding of Peripheral Proteins to Charged Lipid Membranes. *Biophys. J.* **1995**, *68*, 536−546.
(51) Heimburg, T.; Angerstein, B.; Marsh, D. Binding of Peripheral Proteins to Mixed Lipid Membranes: Effect of Lipid Demixing Upon Binding. *Biophys. J.* **1999**, *76*, 2575−2586.
(52) Ladokhin, A. S.; White, S. H. Protein Chemistry at Membrane Interfaces: Non-Additivity of Electrostatic and Hydrophobic Interactions. *J. Mol. Biol.* **2001**, *309*, 543−552.
(53) Seelig, J. Thermodynamics of Lipid-Peptide Interactions. *Biochim. Biophys. Acta* **2004**, *1666*, 40−50.
(54) Hubbuch, J.; Kula, M. R. Confocal Laser Scanning Microscopy as an Analytical Tool in Chromatographic Research. *Bioprocess Biosyst. Eng.* **2008**, *31*, 241−259.
(55) Klocek, G.; Schulthess, T.; Shai, Y.; Seelig, J. Thermodynamics of Melittin Binding to Lipid Bilayers. Aggregation and Pore Formation. *Biochemistry* **2009**, *48*, 2586−2596.
(56) Chatelier, R. C.; Minton, A. P. Adsorption of Globular Proteins on Locally Planar Surfaces: Models for the Effect of Excluded Surface Area and Aggregation of Adsorbed Protein on Adsorption Equilibria. *Biophys. J.* **1996**, *71*, 2367−2374.
(57) Minton, A. P. Adsorption of Globular Proteins on Locally Planar Surfaces. II. Models for the Effect of Multiple Adsorbate Conformations on Adsorption Equilibria and Kinetics. *Biophys. J.* **1999**, *76*, 176−187.
(58) Zuckermann, M. J.; Heimburg, T. Insertion and Pore Formation Driven by Adsorption of Proteins Onto Lipid Bilayer Membrane-Water Interfaces. *Biophys. J.* **2001**, *81*, 2458−2472.
(59) Trusova, V. M.; Gorbenko, G. P.; Sarkar, P.; Luchowski, R.; Akopova, I.; Patsenker, L. D.; Klochko, O.; Tatarets, A. L.; Kudriavtseva, Y. O.; Terpetschnig, E. A.; et al. Förster Resonance Energy Transfer Evidence for Lysozyme Oligomerization in Lipid Environment. *J. Phys. Chem. B* **2010**, *114*, 16773−16782.
(60) Alakoskela, J. M.; Jutila, A.; Simonsen, A. C.; Pirneskoski, J.; Pyhajoki, S.; Turunen, R.; Marttila, S.; Mouritsen, O. G.; Goormaghtigh, E.; Kinnunen, P. K. J. Characteristics of Fibers Formed by Cytochrome c and Induced by Anionic Phospholipids. *Biochemistry* **2006**, *45*, 13447−13453.
(61) Oellerich, S.; Lecomte, S.; Paternostre, M.; Heimburg, T.; Hildebrandt, P. Peripheral and Integral Binding of Cytochrome c to Phospholipids Vesicles. *J. Phys. Chem. B* **2004**, *108*, 3871−3878.
(62) Mulgrew-Nesbitt, A.; Diraviyam, K.; Wang, J. Y.; Singh, S.; Murray, P.; Li, Z. H.; Rogers, L.; Mirkovic, N.; Murray, D. The Role of Electrostatics in Protein-Membrane Interactions. *Biochim. Biophys. Acta* **2006**, *1761*, 812−826.
(63) Hanske, J.; Toffey, J. R.; Morenz, A. M.; Bonilla, A. J.; Schiavoni, K. H.; Pletneva, E. V. Conformational Properties of Cardiolipin-Bound Cytochrome c. *Proc. Natl. Acad. Sci. U.S.A.* **2012**, *109*, 125−130.
(64) Pettersen, E. F.; Goddard, T. D.; Huang, C. C.; Couch, G. S.; Greenblatt, D. M.; Meng, E. C.; Ferrin, T. E. UCSF Chimera - A Visualization System for Exploratory Research and Analysis. *J. Comput. Chem.* **2004**, *25*, 1605−1612.